JGR Space Physics

RESEARCH ARTICLE
10.1029/2023JA031590

Key Points:

- New numerical model of ultra-low-frequency/extremely-low-frequency emission generation in the ionosphere by a near-ground linear current of a finite length has been elaborated
- The model gives the possibility to estimate electromagnetic response of the ionosphere to current sources of different lengths
- Artificial Pc1 pulsations can be generated in the upper ionosphere by a large-scale power line system

Correspondence to:
V. A. Pilipenko,
space.soliton@gmail.com

Citation:
Fedorov, E. N., Mazur, N. G., Pilipenko, V. A., & Vakhnina, V. V. (2023). Generation of artificial ULF/ELF electromagnetic emission in the ionosphere by horizontal ground-based current system. *Journal of Geophysical Research: Space Physics*, *128*, e2023JA031590. https://doi.org/10.1029/2023JA031590

Received 23 APR 2023
Accepted 10 NOV 2023

Author Contributions:
Conceptualization: E. N. Fedorov
Investigation: E. N. Fedorov
Software: N. G. Mazur
Supervision: V. A. Pilipenko
Writing – original draft: V. A. Pilipenko
Writing – review & editing: V. A. Pilipenko

Generation of Artificial ULF/ELF Electromagnetic Emission in the Ionosphere by Horizontal Ground-Based Current System

E. N. Fedorov[1], N. G. Mazur[1], V. A. Pilipenko[1,2], and V. V. Vakhnina[3]

[1]Institute of Physics of the Earth, Moscow, Russia, [2]Geophysical Center, Moscow, Russia, [3]Togliatti State University, Togliatti, Russia

Abstract The feasibility of the detection of electromagnetic response in the upper ionosphere to ground large-scale ultra-low-frequency (ULF) and extremely-low-frequency (ELF) transmitters by low-Earth-orbit (LEO) satellites is considered. As an example of such transmitters, we consider the ZEVS 82 Hz transmitter, FENICS installation driven by 0.5–150 Hz generator, and industrial 50 Hz unbalanced power transmission lines. We numerically model the ULF/ELF wave energy leakage into the upper ionosphere from an oscillating grounded linear power line of a finite length suspended above a ground with a finite resistivity. The numerical scheme is based on the theoretical formalism developed to describe the excitation of an electromagnetic field by a horizontal grounded dipole. A realistic altitudinal profile of the plasma parameters has been reconstructed with the use of the IRI ionospheric model. For the ZEVS transmitter powered by 200 A current the modeled amplitudes of electromagnetic response can reach in the upper nightside ionosphere up to 60 μV/m and 6 pT. The assumption of an infinite source scale overestimates the ionospheric response by a factor of ∼7 as compared with realistic scale 60 km of the ZEVS transmitter. Unbalanced 50 Hz current of 10 A in large-scale (>100 km) power transmission lines can produce the electric response in the upper ionosphere that is sufficient to be detected by electric sensors at LEO satellite. The stimulation of artificial Pc1 pulsations (0.5 Hz) with amplitudes ∼1 pT and ∼10 μV/m by large-scale (>100 km) power lines is possible with driving current >100 A. The use of decommissioned power lines can be a cheap and efficient tool to stimulate Pc1 pulsations in the ionosphere.

Plain Language Summary Our planet was found to exist in an electromagnetic environment, at least in some frequency bands, created by rather industrial activity than by natural processes. The electromagnetic response in the ionosphere to thunderstorms and radio transmitters has been well studied in the very-low-frequency range (>1 kHz), but much less attention has been paid to the extremely-low-frequency (ELF) (≪1 kHz) and ultra-low-frequency (ULF) (<1 Hz) bands. Any noticeable ULF/ELF emission efficiency may be expected only for extremely large-scale emitting systems. Such man-made transmitters do exist. Powerful ELF aerials for communication with submarines with a length of about several tens of km were constructed. Special experiments with controlled sources of electromagnetic fields of ULF/ELF bands were carried out using decommissioned power lines as a horizontal radiating antenna. Transportation systems can also be extended ULF antenna. Finally, unbalanced networks of electric power transmission 50/60 Hz lines become large-scale emitters. Our numerical modeling has proved that manmade ULF/ELF electromagnetic activity near the ground can be monitored by low-Earth-orbit satellites. The large-scale decommissioned power lines can be used to stimulate artificial Pc1 pulsations with frequency ≤1 Hz in the ionosphere-magnetosphere system. These experiments open the possibility to stimulate a loss of relativistic electrons from the radiation belt.

1. Introduction: Large-Scale ELF Transmitters

There appears ever-growing evidence of man-made influence on natural processes in the near-Earth space (Parrot, 2018). This influence was found not only in dedicated active experiments, but also as an unintentional by-product of the technosphere development (Rothkaehl & Parrot, 2005). The electromagnetic response in the ionosphere to natural (e.g., thunderstorms) (Inan et al., 2010) and man-made (e.g., radio transmitters) (Starks et al., 2008) sources has been well studied in the very-low-frequency (VLF) range (>1 kHz). Much less attention has been paid to the ultra-low-frequency (ULF) range (below fundamental Schumann resonance ∼8 Hz) and the extra-low-frequency (ELF) range (above Schumann resonance, but ≪1 kHz). Any noticeable electromagnetic

ULF/ELF radiation efficiency may be expected only from an extremely large-scale emitting system, which really does exist. Powerful aerials for communication with submarines with a length of several tens of km have been constructed in various countries (Bannister et al., 1974). In particular, the transmitter ZEVS operates near the coastline of the White Sea. Controlled sources of electromagnetic fields in ULF/ELF bands using decommissioned power transmission lines as a horizontal radiating antenna were applied for deep magnetotelluric (MT) sounding of the lithosphere (Boerner, 1992; Velikhov et al., 1998). All industrial regions of the Earth are covered by networks of three-phase electric power transmission lines extended to many hundreds of km. If the transmitted currents are unbalanced for some reason, these power lines become large-scale emitters. Rail transportation systems also can be the source of ULF/ELF electromagnetic disturbances. For example, power for trains in California is provided by a 1,000 V rail with a total length of 270 km. Large fluctuating currents (5–10 kA) that flow in this rail make the entire train system a large ULF antenna (Fraser-Smith & Coates, 1978).

Electromagnetic disturbances and emissions from large-scale systems can be observed at vast territories and even leak into the outer space. The most ubiquitous type of electromagnetic radiation emanating from the Earth is the 50/60 Hz power line emission (PLE). PLEs were discovered in the upper ionosphere at the fundamental frequency and its third harmonic above highly industrialized regions in low-Earth-orbit (LEO) satellite missions (Pilipenko et al., 2021; Zhang & Ma, 2018). The PLE intensities recorded during magnetically disturbed periods were systematically larger than the intensities during low activity, and the nighttime overall intensities were considerably larger than the daytime intensities (Nemec et al., 2015). The DEMETER satellite observations revealed that an amount of global emitted energy by transmission lines has been ever increasing in time since the world's total electric generation power increases. Moreover, a sudden increase in the number of PLE events was especially noticeable since extra-high-voltage (EHV) and ultra-high-voltage (UHV) transmission projects started to develop rapidly (Wu, Guo, Yan, & Zhang, 2019). Geographic maps of the statistical PLE occurrence rate derived from DEMETER observations showed a remarkable agreement with the world map of power consumption (Nemec et al., 2015). Even the leakage of PLE from EHV/UHV transmission lines into conjugated ionosphere was observed (Wu et al., 2022). Power lines can be an effective emitter not only of 50/60 Hz PLE, but of power line harmonic radiation (PLHR) at very high harmonics, about 1 kHz (Nemec et al., 2008; Wu et al., 2014; Wu, Guo, Yue, et al., 2019). In this frequency range a power line can efficiently operate as a Beverage antenna (Kostrov et al., 2017), which explains the ubiquity of PLHR observations in space.

The information about penetration into space of ELF emission from other large-scale systems is very sparse. The 82 Hz emission was detected by the DEMETER satellite during overflights above the ZEVS transmitter (Parrot, 2018; Pilipenko et al., 2019). No attempt to detect ULF/ELF emissions in space during experiments with controlled MT sources were performed yet.

Electromagnetic field propagation from an ELF emitting dipole along the Earth-ionosphere waveguide has been well-modeled theoretically (Bernstain et al., 1974; Ermakova et al., 2021; Nickolaenko et al., 2016; Sobchakov et al., 2003; Tereshenko & Tereshenko, 2017). In these works, the ionosphere was modeled as a conductive homogeneous layer or an impedance wall. The wave leakage into the ionosphere is small and such simplified models are quite adequate for the description of the ELF wave long-distance propagation in the waveguide Earth—bottom ionosphere. Besides submarine communication, a great stimulus for such studies was provided by experiments with controlled sources of electromagnetic fields in ULF/ELF bands for MT sounding using a power transmission line as a horizontal radiating antenna (Zhamaletdinov et al., 2015). The artificial ULF-ELF signals were detected at large distances from the emitter (Belyaev et al., 2002; Ermakova et al., 2006).

At the same time, the ULF/ELF wave energy transmission from ground sources toward LEO has not been adequately examined with a realistic ionospheric model. In contrast to VLF emitters (like radio transmitters or lightning strokes) a source of ULF/ELF emissions cannot be imagined as a point dipole, but its finite scale, often exceeding the height of the lower ionosphere (~100 km), must be taken into account. As a first step, Fedorov et al. (2020) presented a numerical model of electromagnetic response of a realistic ionosphere in the vertical geomagnetic field $\mathbf{B}_0$ to a near-ground infinite linear current. An altitudinal profile of the plasma parameters has been reconstructed with the use of the International Reference Ionosphere (IRI) model (Bilitza et al., 2022). This theoretical model was generalized in Fedorov et al. (2021) by consideration of an arbitrary geomagnetic field inclination and power line orientation. The account for a geomagnetic field inclination makes the problem significantly more complicated because the medium parameters become axially nonsymmetric. The elaborated numerical model for a mid-latitude ionosphere with an inclined $\mathbf{B}_0$ showed that PLE energy is partially guided by

geomagnetic field lines, so the maximal intensity in the upper ionosphere is shifted equatorward from a vertical and diminishes upon the latitude decrease, but not significantly.

In this paper, we further investigate theoretically the efficiency of the ULF/ELF wave excitation in the upper ionosphere by a linear near-Earth grounded power line, but of a finite length. The mathematical basis for this numerical model has been developed in Fedorov et al. (2023). On the basis of this mathematical formalism, we have elaborated a numerical model with a realistic ionospheric profile. A special attention has been paid to the dependence of maximal emission intensity on the length of a near-ground emitter and frequency. The expected wave amplitude at LEO for various types of ELF transmitters has been calculated.

2. Possible ELF Sources

Oppositely to standard radio transmitters, the generation of artificial signals in the ULF-ELF range needs specific large-scale devices to be efficient. To communicate with submarines below water and ice, the ELF transmitter ZEVS on the Kola Peninsula was deployed. ZEVS consists of two parallel horizontal grounded antennas about 60 km in length that emits at frequency 82 Hz (Velikhov et al., 1994). The transmitter lines are elongated nearly in the East-West direction at the latitude 68°48′N. The generator pumps in the antenna a current up to 200–300 A and power up to 2.5 MW.

The experiments FENICS (Fennoscandian Electrical conductivity from soundings with the Natural and Controlled Sources) for MT studies are conducted regularly on the Kola Peninsula with the use of two power transmission lines with length $L = 100$ km and $L = 120$ km as controlled ULF-ELF emitters (Zhamaletdinov et al., 2015). During the experiments the generator with a power of 200 kW yields in power lines the alternating current (AC) with amplitude from 240 A at low frequencies (<10 Hz) to 20 A at higher frequencies (∼200 Hz).

All industrial regions are covered by networks of electric power transmission lines extended to many hundreds of km. Under ideal conditions, a three-phase power transmission line must be balanced (symmetrical), that is, the voltage and current of each phase have the same amplitude, and the shift between phases is exactly 120°. If at least one of these conditions is not met, then a system becomes unbalanced (asymmetrical). Such imbalance leads to a decrease in the efficiency of a transmission line and power losses due to the radiation of electromagnetic energy. In most cases, the source of the imbalance is the asymmetry of the load (high-speed railways, metallurgy induction furnaces, computer data centers, etc.). Substantial distortions in the power line operation can be produced by geomagnetically induced currents (GICs) caused by rapid variations of the geomagnetic field, that is, high dB/dt values (see review (Pilipenko, 2021)). The detection of PLE at large distances from a three-phase power line may be considered as an indicator of its unbalanced operation.

3. Modeling the Electromagnetic Field of a Horizontal Grounded Current Line Situated Above a Conducting Ground

The presented numerical model considers the multi-layered horizontally homogeneous medium with a realistic ionospheric vertical profile. The model of the medium is similar to the model used for the description of ULF transients in the ionosphere produced by lightning discharges (Fedorov et al., 2016; Mazur et al., 2018), whereas the sources, basic equations, and solution techniques are different.

We consider electromagnetic field only in the vicinity of the transmitter (about several hundred km and less). For such distances, the plane geometry is a good approximation. The axis Z of the Cartesian coordinate system is chosen to be vertical upward with $z = 0$ on the ground, whereas the axis X is along the current, and Y is across the current. For simplicity, the geomagnetic field is assumed to be vertical (the geomagnetic field inclination $I = 90°$). We assume that the electromagnetic field is excited by a linear current $J(t) = J_0 \exp(-i\omega t)$, situated at a small altitude above the Earth's surface and oscillating with frequency ω. However, in contrast with previous studies, the length of emitting line L is considered as finite one.

Upon modeling of the linear power line suspended above the Earth's surface and grounded at the ends, it is necessary to take into account the spreading electric currents inside the Earth. The easiest way to do this is to shift formally the current down into the Earth to a small depth (about a few meters), as illustrated in Figure 1. This small downward shift of the antenna has no effect on the field in the atmosphere and ionosphere, but reduces

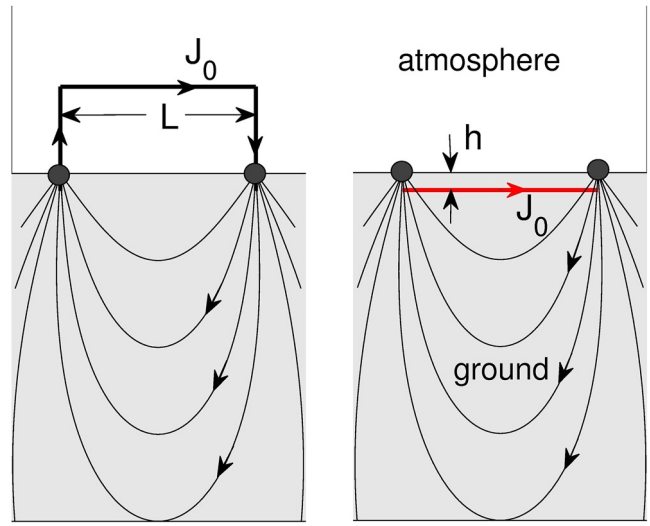

Figure 1. Sketch of the problem geometry. Illustration of modification from a grounded line with current intensity J_0 and length L suspended above ground with finite conductivity σ_g to a line beneath the Earth's surface at small depth h.

the problem to a much simpler geometrical consideration. This approach automatically accounts for the electric current spreading in the crust, as justified in Fedorov et al. (2023).

We search magnetic $\mathbf{B}(x, y, z, t)$ and electric $\mathbf{e}(x, y, z, t) \equiv c^{-1}\mathbf{E}$ fields (c is light velocity) as a time harmonic $\propto \exp(-i\omega t)$, and solve Maxwell's equations with the external driving current density $\mathbf{j}$

$$\nabla \times \mathbf{B} = -ik_0\hat{\boldsymbol{\varepsilon}}\mathbf{e} + \mu_0\mathbf{j}, \qquad \nabla \times \mathbf{e} = ik_0\mathbf{B}, \tag{1}$$

where $k_0 = \omega/c$ is the wave number in free space. The tensor of relative dielectric permeability of the ionospheric plasma $\hat{\boldsymbol{\varepsilon}} = \boldsymbol{\varepsilon}/\varepsilon_0$ (where ε_0 is the vacuum dielectric permeability) in the chosen coordinate system with the field-aligned axis Z has the form

$$\hat{\boldsymbol{\varepsilon}} = \begin{pmatrix} \varepsilon_\perp & ig & 0 \\ -ig & \varepsilon_\perp & 0 \\ 0 & 0 & \varepsilon_\parallel \end{pmatrix}.$$

The standard formulas for the elements of the tensor $\boldsymbol{\varepsilon}$ in a collisional plasma can be found elsewhere (e.g., Wait, 1972). In the near-Earth atmosphere the tensor elements are reduced to $\varepsilon_\perp = \varepsilon_\parallel = 1$ and $g = 0$.

The first step in solving the problem is to find a solution of Maxwell's equations with a source as a point horizontal current (current dipole). This formalism is detailed below in Section 3.2, where the specific form of Maxwell's equations is given for this particular case. Having found a solution for such an elementary source, at the next step it is easy to calculate the total field, excited by a horizontal current of a finite length, just summarizing the fields generated by elementary current dipoles.

3.1. Equations for the Wave Potentials

We use the representation of electromagnetic field via the wave potentials. In this formalism, in the horizontal plane z = const the field of a driving current density is split into a curl-free and divergence-free (vortex) components, generating TE (transverse electric) modes and TM (transverse magnetic) modes, correspondingly. This division is fundamental in solving the problem under consideration. The initial problem is obviously devoid of axial symmetry, while it turns out that field components generated by the curl-free and vortex components of the driving current separately have such symmetry. Thanks to this, it becomes possible to separate variables using

Hankel's transform and come to boundary problems for a system of ordinary differential equations (ODEs) separately for curl-free and vortex components of the driving current.

The electric and magnetic fields are standardly represented through scalar Φ and vector $\mathbf{A}$ potentials as follows: $\mathbf{B} = \nabla \times \mathbf{A}$ and $\mathbf{e} = -\nabla\Phi + ik_0\mathbf{A}$. Using the calibration condition $\nabla_\perp \cdot \mathbf{A}_\perp = 0$ the transverse component of the vector potential can be represented in the form $\mathbf{A}_\perp = (ik_0)^{-1}\nabla \times \Psi\hat{\mathbf{z}}$, where Ψ is the scalar potential. Thus, we arrive at the following representation of the electromagnetic field via three potentials A, Φ, and Ψ.

$$\mathbf{B} = \nabla A \times \hat{\mathbf{z}} + (ik_0)^{-1}\nabla_\perp \partial_z \Psi - (ik_0)^{-1}\nabla_\perp^2 \Psi\hat{\mathbf{z}}, \tag{2}$$

$$\mathbf{e} = -\nabla\Phi + ik_0 A\hat{\mathbf{z}} + \nabla\Psi \times \hat{\mathbf{z}}. \tag{3}$$

From Maxwell's Equation 1 and expressions (2) and (3) the system of partial differential equations (PDEs) describing these potentials follows (Fedorov et al., 2023)

$$\begin{aligned} \nabla_\perp^2 \partial_z A &= ik_0\varepsilon_\perp \nabla_\perp^2 \Phi + k_0 g\, \nabla_\perp^2 \Psi + \mu_0 \operatorname{Div} \mathbf{j}_\perp, \\ \nabla_\perp^2 \left(\partial_z^2 + \nabla_\perp^2 + k_0^2\varepsilon_\perp\right)\Psi &= -ik_0^2 g\, \nabla_\perp^2 \Phi + ik_0\mu_0 \operatorname{Curl} \mathbf{j}_\perp, \\ \partial_z \Phi &= ik_0\left[1 + \left(k_0^2\varepsilon_\parallel\right)^{-1}\nabla_\perp^2\right]A - (ik_0\varepsilon_\parallel)^{-1}\mu_0 j_\parallel. \end{aligned} \tag{4}$$

Here 2D operators $\operatorname{Div} \mathbf{a} = \partial_x a_x + \partial_y a_y$ and $\operatorname{Curl} \mathbf{a} = \partial_x a_y - \partial_y a_x$ have been used.

3.2. Field of a Horizontal Current Dipole

Now we study the field produced by a horizontal current element directed along the axis X and located at height $z = h < 0$ with a length d which is much less than the distance to the observation point. Such an elementary source may be considered as a current dipole with the moment M_0. The driver current density in Equation 4 for such a source has the components $j_\parallel = 0$, and $\mathbf{j}_\perp = j_x\hat{\mathbf{x}} = M_0\delta(x)\delta(y)\delta(z-h)\hat{\mathbf{x}}$. Now, taking into account the further transition to the cylindrical coordinates ϱ, φ, z and subsequent transformation of the equations, it is convenient to present the horizontal component as

$$j_x(x, y, z) = M_0\pi^{-1}\varepsilon^{-2}\exp\left(-\varrho^2/\varepsilon^2\right)\delta(z-h) \qquad \left(\varrho^2 = x^2 + y^2\right),$$

which tends to $M_0\delta(x)\delta(y)\delta(z-h)$ at $\varepsilon \to 0$. Thus, the source terms in the right-hand parts of (Equation 4) for current dipole case in the cylindrical coordinates are as follows

$$\operatorname{Div} \mathbf{j}_\perp = q_\varepsilon(\varrho)\delta(z-h)\cos\varphi, \quad \operatorname{Curl} \mathbf{j}_\perp = -q_\varepsilon(\varrho)\delta(z-h)\sin\varphi, \tag{5}$$

where $q_\varepsilon(\varrho) = M_0\partial_\varrho[\pi^{-1}\varepsilon^{-2}\exp(-\varrho^2/\varepsilon^2)]$. Only a curl-free part of the driving current contributes into the source term $\operatorname{Div} \mathbf{j}_\perp$, while the vortex component of the current contributes into $\operatorname{Curl} \mathbf{j}_\perp$. The solution of system (Equation 4) with such specific form of driver terms is searched in the form $F(\varrho, \varphi, z) = F_c(\varrho, z)\cos\varphi + F_s(\varrho, z)\sin\varphi$, where $F = A, \Phi, \Psi$. Substituting these combinations into (Equation 4) and grouping terms with factors $\cos\varphi$ and $\sin\varphi$, the following system is obtained (Fedorov et al., 2023)

$$\begin{aligned} \partial_z A_{c,s} &= ik_0\varepsilon_\perp \Phi_{c,s} + k_0 g\Psi_{c,s} + a_{c,s}, \\ \partial_z B_{c,s} &= -k_0 g\Phi_{c,s} - (ik_0)^{-1}\left(k_0^2\varepsilon_\perp + \mathrm{R}\right)\Psi_{c,s} - b_{c,s}, \\ \partial_z \Phi_{c,s} &= ik_0\left[1 + \left(k_0^2\varepsilon_\parallel\right)^{-1}\mathrm{R}\right]A_{c,s}, \\ \partial_z \Psi_{c,s} &= ik_0 B_{c,s}. \end{aligned} \tag{6}$$

Here the operator $\mathrm{R} = \varrho^{-1}\partial_\varrho\varrho\partial_\varrho - \varrho^{-2}$, the inhomogeneous terms are $a_c = b_s = \mu_0 \mathrm{R}^{-1} q_\varepsilon(\varrho)\delta(z-h)$, and $a_s = b_c = 0$. For symmetry the additional function $B_{c,s} = (ik_0)^{-1}\partial_z \Psi_{c,s}$ has been introduced.

It is of fundamental importance that system (Equation 6) has a cylindrical symmetry, thus the asymmetry of the original problem has been overcome thanks to splitting into two components having different angular dependence ($\propto \cos\varphi$ and $\propto \sin\varphi$). This gives the possibility to separate variables and arrive at 1D boundary value problem. System (Equation 6) of PDEs is further reduced to the system of ODEs in respect to the variable z using the Hankel's transform of the 1st order. This transform $\mathbb{K}_1[f(\varrho)](k)$ reduces the differential operator R to simple

multiplication by $-k^2$. For this reason the coefficients of system (Equation 6) experience a very simple transformation, and some explanation requires only the inhomogeneous terms $a_c = b_s$ reduction. Applying the transform $\mathbb{K}_1$ to $a_c = b_s = \mu_0 \mathrm{R}^{-1} q_e(\varrho)\delta(z-h)$ we obtain $-k^{-2}\mu_0 M_0 \pi^{-1}\varepsilon^{-2}\delta(z-h)\mathbb{K}_1\left[\partial_\varrho\left(\exp\left(-\varrho^2/\varepsilon^2\right)\right)\right]$. Here the property of transform $\mathbb{K}_1[f(\varrho)](k)$ is used that it reduces the differential operator R to simple multiplication by $-k^2$, so R^{-1} is reduced to multiplication by $-k^{-2}$. Further, we find

$$\mathbb{K}_1\left[\partial_\varrho\left(\exp\left(-\varrho^2/\varepsilon^2\right)\right)\right] = \int_0^\infty \varrho J_1(k\varrho)\partial_\varrho\left(\exp\left(-\varrho^2/\varepsilon^2\right)\right)d\varrho =$$

$$-\int_0^\infty \exp\left(-\varrho^2/\varepsilon^2\right)\partial_\varrho\left(\varrho J_1(k\varrho)\right)d\varrho = -\int_0^\infty \exp\left(-\varrho^2/\varepsilon^2\right)\partial_\varrho\left(\frac{1}{2}k\varrho^2 + O\left(\varrho^4\right)\right)d\varrho = -\frac{k\varepsilon^2}{2} + O\left(\varepsilon^4\right),$$

and, finally, $\mathbb{K}_1[a_c(\rho)] = \mathbb{K}_1 b_s(\rho)] = k^{-1}\mu_0 M_0 (2\pi)^{-1}\delta(z-h) + O\left(\varepsilon^2\right)$ at $\varepsilon \to 0$. Taking this into account while applying the transform $\mathbb{K}_1$ to Equation 6, and introducing new variables $\tilde{A}_{c,s} = k\mathbb{K}_1\left[A_{c,s}\right]$, $\tilde{B}_{c,s} = k\mathbb{K}_1\left[B_{c,s}\right]$, $\tilde{\Phi}_{c,s} = k\mathbb{K}_1\left[\Phi_{c,s}\right]$, and $\tilde{\Psi}_{c,s} = k\mathbb{K}_1\left[\Psi_{c,s}\right]$ (where multiplication with k is used to remove the singularity k^{-1}), we arrive at the system of ODEs

$$\begin{aligned} \partial_z \tilde{A}_{c,s} &= \alpha\tilde{\Phi}_{c,s} + \beta\tilde{\Psi}_{c,s} + \tilde{a}_{c,s}, \qquad \partial_z \tilde{\Phi}_{c,s} = \lambda\tilde{A}_{c,s}, \\ \partial_z \tilde{B}_{c,s} &= \gamma\tilde{\Phi}_{c,s} + \delta\tilde{\Psi}_{c,s} - \tilde{b}_{c,s}, \qquad \partial_z \tilde{\Psi}_{c,s} = ik_0\tilde{B}_{c,s}. \end{aligned} \tag{7}$$

Here $\alpha = ik_0\varepsilon_\perp, \beta = k_0 g, \gamma = -k_0 g, \delta = ik_0\left(\varepsilon_\perp - k^2/k_0^2\right), \lambda = ik_0\left[1 - k^2/\left(k_0^2\varepsilon_\parallel\right)\right], \tilde{a}_c = \tilde{b}_s = (2\pi)^{-1}\mu_0 M_0\delta(z-h)$, and $\tilde{a}_s = \tilde{b}_c = 0$. Also the terms $O(\varepsilon^2)$ here are neglected.

System (Equation 7) is to be augmented with boundary conditions at $z \to \pm\infty$. It is natural to assume that the electromagnetic field decreases upon an uplift into the ionosphere and immersion into the ground. The numerical solution scheme of the boundary problem under consideration for system (Equation 7) was presented in detail in Fedorov et al. (2023), so here just a brief description of this procedure is given. The occurrence of the factor $\delta(z-h)$ in the inhomogeneous terms of system (Equation 7) makes it equivalent to a homogeneous system with the matching condition at $z = h$. This condition can be obtained by integration of (Equation 7) across the source, that is from $z = h - 0$ to $z = h + 0$. The homogeneous system corresponding to system (Equation 7) can be presented in a vector form as

$$\partial_z \mathbf{u} = \mathbf{S}\mathbf{v}, \qquad \partial_z \mathbf{v} = \mathbf{T}\mathbf{u}, \tag{8}$$

using 2D vectors $\mathbf{u} = \left(\tilde{A}_{c,s}, \tilde{B}_{c,s}\right)$, $\mathbf{v} = \left(\tilde{\Phi}_{c,s}, \tilde{\Psi}_{c,s}\right)$, and 2×2 matrices $\mathbf{S}$ and $\mathbf{T}$ of the coefficients in Equation 7. It is helpful to introduce the matrix $\mathbf{Y}(z)$, which transforms the vector $\mathbf{v}(z)$ into the vector $\mathbf{u}(z)$ as follows: $\mathbf{u}(z) = \mathbf{Y}(z)\mathbf{v}(z)$. This matrix is similar to the impedance matrix relating electric and magnetic components (Budden, 1985). The introduction of the impedance matrix facilitates the solution of Maxwell's equations upon appearance of fast growing or decaying wave modes. The matrix $\mathbf{Y}(z)$ obeys the nonlinear differential equation of the Riccati type

$$\partial_z \mathbf{Y} = \mathbf{S} - \mathbf{Y}\mathbf{T}\mathbf{Y}. \tag{9}$$

The boundary conditions for system (Equation 7) determine unambiguously the limiting values of the matrix $\mathbf{Y}$ at $z \to \pm\infty$. Therefore, one can calculate $\mathbf{Y}(z)$ by numerical solution of Equation 9 from above and from below to the source location and obtain different values $\mathbf{Y}(h \pm 0)$ there. Combining this discontinuity with matching conditions at the source altitude $z = h$ for system (Equation 8) one can find the limiting values of the vectors $\mathbf{u}(h \pm 0)$ and $\mathbf{v}(h \pm 0)$. Using them as the boundary values for a numerical solution of Cauchy problem for system (Equation 8) upwards and downwards from the source level we get a solution of Equation 7 at any height z. A detailed description of the above procedure is given in Fedorov et al. (2023).

Finally, when the solution of system (Equation 7) has been obtained, we apply to it the inverse Hankel's transform and use the relationships (Equation 3) (transformed to cylindrical coordinates). As a result the following relationships for the components of total field are obtained

$$
\begin{aligned}
B_\varrho &= \cos\,\varphi\left(\varrho^{-1}(A_s - B_c) + \mathbb{K}_0\left[\tilde{B}_c\right]\right) - \sin\,\varphi\left(\varrho^{-1}(A_c + B_s) - \mathbb{K}_0\left[\tilde{B}_s\right]\right),\\
B_\varphi &= \cos\,\varphi\left(\varrho^{-1}(A_c + B_s) - \mathbb{K}_0\left[\tilde{A}_c\right]\right) + \sin\,\varphi\left(\varrho^{-1}(A_s - B_c) - \mathbb{K}_0\left[\tilde{A}_s\right]\right),\\
B_z &= (ik_0)^{-1}\left(\cos\,\varphi\,\mathbb{K}_1\left[k\tilde{\Psi}_c\right] + \sin\,\varphi\,\mathbb{K}_1\left[k\tilde{\Psi}_s\right]\right),\\
e_\varrho &= \cos\,\varphi\left(\varrho^{-1}(\Phi_c + \Psi_s) - \mathbb{K}_0\left[\tilde{\Phi}_c\right]\right) + \sin\,\varphi\left(\varrho^{-1}(\Phi_s - \Psi_c) - \mathbb{K}_0\left[\tilde{\Phi}_s\right]\right),\\
e_\varphi &= \cos\,\varphi\left(\varrho^{-1}(\Psi_c - \Phi_s) - \mathbb{K}_0\left[\tilde{\Psi}_c\right]\right) + \sin\,\varphi\left(\varrho^{-1}(\Psi_s + \Phi_c) - \mathbb{K}_0\left[\tilde{\Psi}_s\right]\right),\\
e_z &= i(k_0\varepsilon_\parallel)^{-1}\left(\cos\,\varphi\,\mathbb{K}_1\left[k\tilde{A}_c\right] + \sin\,\varphi\,\mathbb{K}_1\left[k\tilde{A}_s\right]\right).
\end{aligned}
$$

Here $A_{c,s} = \mathbb{K}_1\left[k^{-1}\tilde{A}_{c,s}\right]$, $B_{c,s} = \mathbb{K}_1\left[k^{-1}\tilde{B}_{c,s}\right]$, $\Phi_{c,s} = \mathbb{K}_1\left[k^{-1}\tilde{\Phi}_{c,s}\right]$, and $\Psi_{c,s} = \mathbb{K}_1\left[k^{-1}\tilde{\Psi}_{c,s}\right]$. The Hankel's transforms of the zero-th and first order, $\mathbb{K}_0$ and $\mathbb{K}_1$, have been used.

3.3. Field of the Finite-Length Current

Let a line current with amplitude J_0 and length L be situated at the segment $-L/2 \le x \le L/2$. To find the electromagnetic field generated by this finite-length current we use the results for a current dipole presented in Section 3.2. Let us set a large number N of such elementary dipoles with the moment $M_0 = J_0 d$ to the middle of N subsegments. The total current corresponding to such a system of dipoles is $J_0 = NM_0L^{-1}$. A discrete structure of such system of elementary currents reveals itself only at small distances $\le d = L/N$.

The calculation of the fields $\mathbf{B}(x, y, z)$ and $\mathbf{e}(x, y, z)$ produced by this set of horizontal current dipoles is as follows. The cylindrical coordinates $\varrho_n(x, y)$ and $\varphi_n(x, y)$ of the observation point (x, y, z) with respect to nth dipole are $\varrho_n = \left[(x - x_n)^2 + y^2\right]^{1/2}$ and $\varphi_n = \arcsin\left(y\varrho_n^{-1}\right)$. Substituting these values into the formulas for a current dipole presented above, we obtain the components of the field produced by nth dipole: $B^{(n)}_{\varrho,\varphi,z}(x, y, z) = B_{\varrho,\varphi,z}(\varrho_n, \varphi_n, z)$ and $e^{(n)}_{\varrho,\varphi,z}(x, y, z) = e_{\varrho,\varphi,z}(\varrho_n, \varphi_n, z)$. The horizontal components are to be transformed by the corresponding rotation to the coordinate system with axes X, Y: $B^{(n)}_{\varrho,\varphi}(x, y, z) \to B^{(n)}_{x,y}(x, y, z)$ and $e^{(n)}_{\varrho,\varphi}(x, y, z) \to e^{(n)}_{x,y}(x, y, z)$; the vertical components need no such transformation. Finally, these fields from all dipoles are summed up to determine the total field generated by the finite-length line current.

4. Application to the Analysis of Electromagnetic Emission Produced by Grounded ELF Transmitters

The IRI model is the most validated and widespread model of a standard ionosphere, which provides for any location on Earth and time moment the vertical profile of main ionospheric constituents. The IRI parameters have been chosen, rather arbitrarily, for the winter nighttime conditions (LT = 21, 2007/12/08) and geographic latitude 69° corresponding to the ZEVS/FENICS location. The IRI-derived static Pedersen and Hall conductances are $\Sigma_P = 0.04$ S, $\Sigma_H = 0.12$ S; the density peak height is $h_mF2 = 303$ km, and the total ionospheric content (integration from 50 to 2,000 km) is 0.5 TECu. The ZEVS/FENICS installations are located at a crystalline shield with a high resistance, so for calculations we have used a typical upper crust conductivity in this region $\sigma_g = 10^{-5}$ S/m. The atmospheric conductivity is taken to be $\sigma_a = 1.1 \cdot 10^{-14}$ S/m near the ground surface and increases exponentially to an altitude of 80 km to match the IRI-deduced conductivity. According to the IGRF geomagnetic model, the magnetic field inclination at the ZEVS/FENICS location is $I = 78°$. Because the deviation from the vertical magnetic field is small, we assume that $I = 90°$. The same ionospheric and geoelectric parameters are used for the modeling of power transmission lines.

The calculated field components are normalized to the permanent source current $J_0 = 1$ A. The excited field is estimated at a fixed altitude ($z = 660$ km) corresponding to the DEMETER orbit. The magnitude of the electromagnetic field in the ionosphere is characterized by amplitudes of the large semi-axis of the polarization ellipse, $\max|\mathbf{E}|$ and $\max|\mathbf{B}|$.

4.1. ZEVS Transmitter

In earlier papers (Fedorov et al., 2020; Pilipenko et al., 2019) the source current was supposed to be infinitely long. This assumption probably overestimated the effect of a realistic current with a finite length, but how severely? To answer this question, we have calculated the electric field in the upper ionosphere excited by the grounded emit-

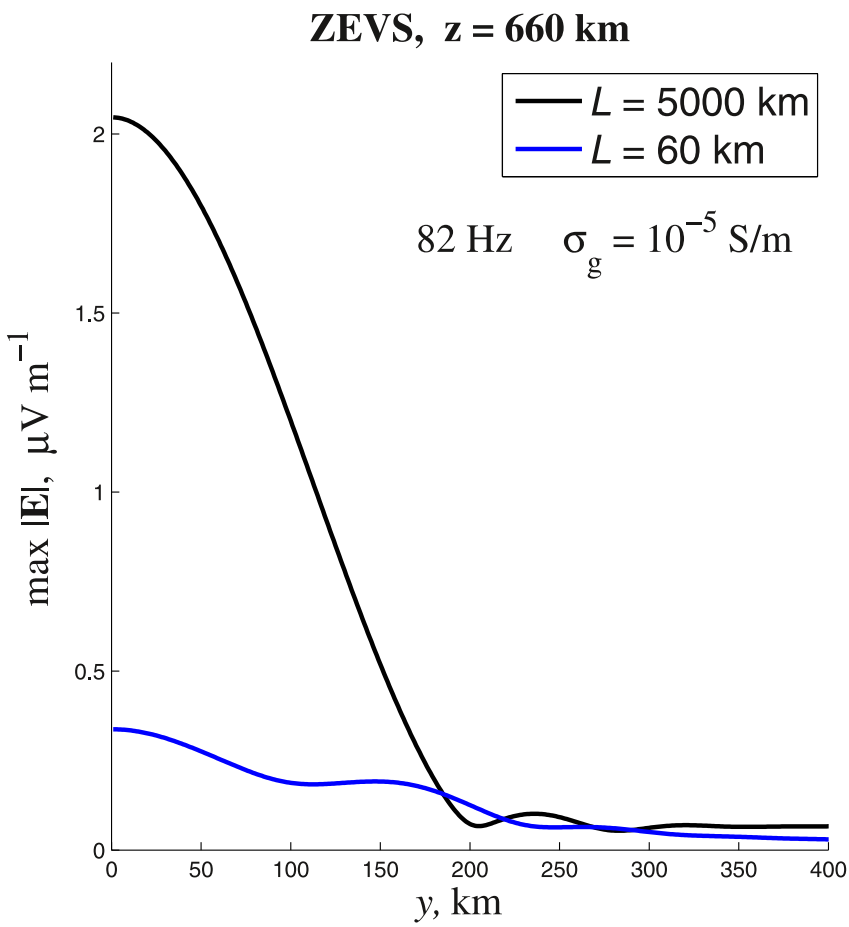

Figure 2. The radial structure of the electric field magnitude max|**E**| of electromagnetic emission in the direction across the antenna ($\phi = \pi/2$) in the upper nighttime ionosphere ($z = 660$ km) generated by linear current oscillators at $f = 82$ Hz with $J_0 = 1$ A for $L = 60$ km and $L = 5{,}000$ km.

ters with $f = 82$ Hz and different lengths. Figure 2 shows the spatial structure in the direction across the antenna of the electric field generated by a very large-scale source ($L = 5{,}000$ km) and realistic source ($L = 60$ km). For an extended source (which practically corresponds to the infinite line model) the electric field reaches above the source ($y = 0$) the magnitude ~2.1 μV/m. For the emitter with a scale of 60 km, the amplitude reaches only ~0.3 μV/m. Thus, the assumption of an infinite scale overestimates the E-field in the upper ionosphere by a factor of ~7 as compared with the realistic scale of the ZEVS transmitter. The field decrease from a source is not very fast, so upon separation by ~200 km from the vertical above the source, the amplitude drops only by a factor of ~2 (Figure 6). At larger distances ($\rho > 200$ km), the difference between fields from the infinite and finite-scale currents becomes nonsignificant.

The transverse magnetic field $|\mathbf{B}_H|$ in the upper ionosphere can reach up to $\sim 3.5 \cdot 10^{-2}$ pT for ZEVS emitter (Figure 3). The spatial structure of $|\mathbf{B}_H|(\rho)$ is roughly the same for the direction along the current ($\varphi = 0$) and across it ($\varphi = 90°$).

The radiation pattern of the excited E-field in various directions, measured by the azimuthal angle φ, is shown in Figure 4. Above the source ($\rho = 20$ km) the radiation pattern is slightly elliptical. The largest |**E**| field is observed in the middle of quadrant (at $\varphi \simeq 45°$), where $|E_x| \approx |E_y|$. Upon increase of distance ($\rho = 240$ km) the emission becomes nearly isotropic. Thus, though the primary source is linear, the emission transmitted into the ionosphere is nearly isotropic in the horizontal plane.

According to the modeling results, the ZEVS transmitter with a realistic current $J_0 = 200$ A can produce the maximal response in the upper nightside ionosphere up to ~60 μV/m and ~7 pT. Such amplitudes can be detected

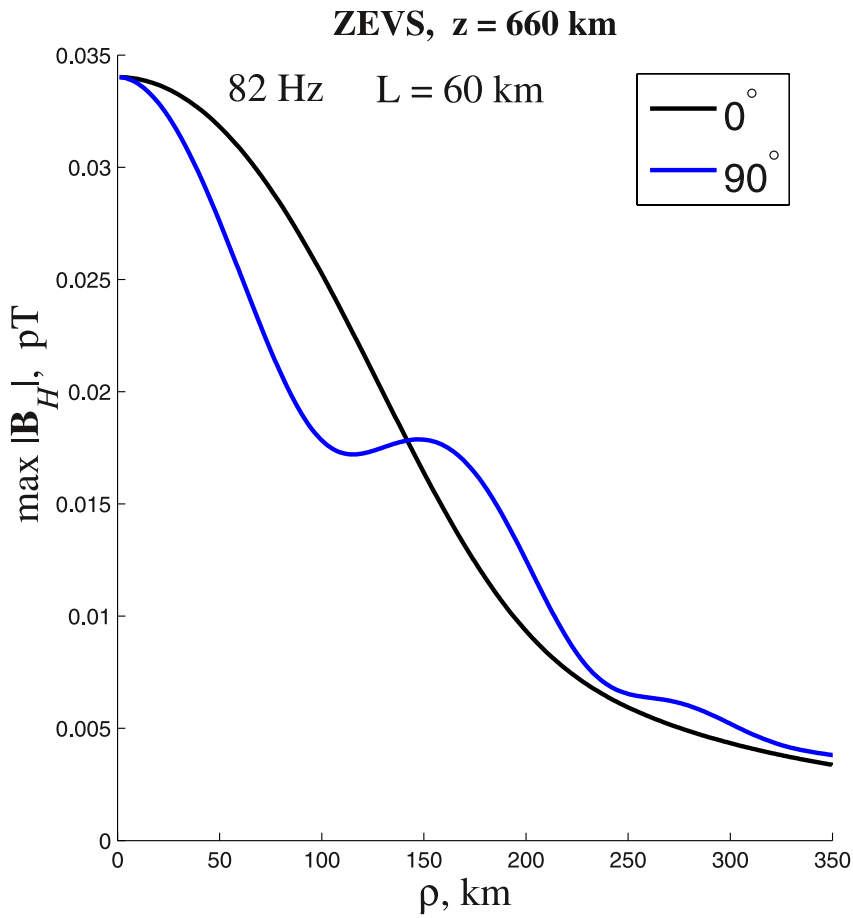

Figure 3. The radial structure of the magnitude of the horizontal magnetic field max $|\mathbf{B}_H|$ of electromagnetic emission generated by 82 Hz transmitter with length $L = 60$ km and $J_0 = 1$ A. The azimuthal angle φ is measured from the X axis counterclockwise (0° – along the antenna, 90° – across the antenna).

by a LEO satellite. Indeed, the DEMETER satellite recorded 82 Hz emission above Kola Peninsula with power spectral density of electric component $\log_{10} W_E \simeq 1.0-3.5$ $(\mu V/m)^2/Hz$ and magnetic component $\log_{10} W_B \simeq -(5.5-6.0)$ nT^2/Hz (Pilipenko et al., 2019).

4.2. FENICS Installation

Now we consider the ULF/ELF emission intensity that may be observed in the upper ionosphere above the FENICS installation ($L = 100$ km). The spatial structure of the emission intensity max $|\mathbf{E}|$ in the direction across the antenna for various emission frequencies is shown in Figure 5. Just above the installation ($y = 0$) the wave transmission into the ionosphere becomes better with an increase of frequency: upon growth of f from 3 to 150 Hz the E-field increases from ~0.25 μV/m to ~0.8 μV/m.

In general, for the frequency band 10–150 Hz above the FENICS installation the electric field amplitude reaches max $|\mathbf{E}| \sim 0.3-0.8$ μV/m. Thus, for typical current $J_0 = 100$ A during previous FENICS experiments, the ELF emissions in this band can leak into the upper ionosphere with amplitudes up to ~30–80 μV/m. Such magnitudes could be detected by electric sensors on modern LEO satellites. However, any attempt to detect the response in space to FENICS or any other ULF/ELF experiment with power lines as a controlled source has not been undertaken yet.

4.3. Power Lines of Different Lengths

Now we consider how the amplitude of 50 Hz PLE in the upper ionosphere varies depending on the linear scale of a transmission line with an unbalanced current $J_0 = 1$ A. Comparison of the PLE amplitudes for various

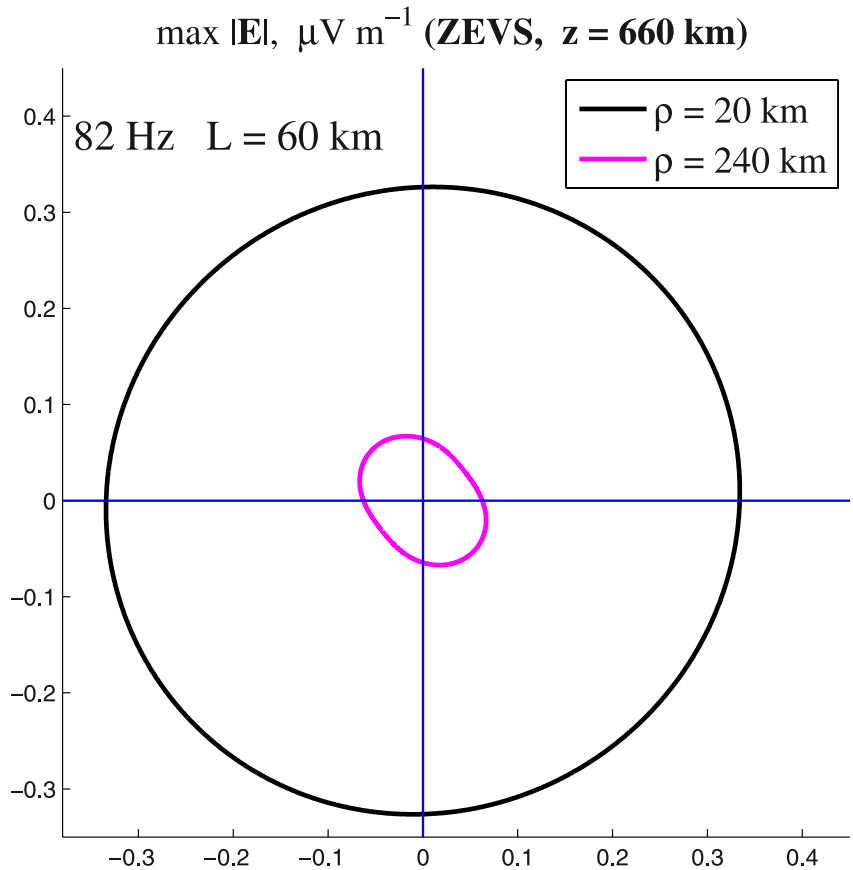

Figure 4. The ZEVS radiation pattern ($f = 82$ Hz) in the upper ionosphere ($z = 660$ km)—the angular distribution of the electric component magnitude at two horizontal distances from the emitter.

line lengths L is given in Figure 6. Just above ($y = 0$) large-scale line with $L = 500$ km the electric component amplitude reaches $|\mathbf{E}| \simeq 1.9$ μV/m. Upon decrease of the line length the intensity of PLE in the upper ionosphere decreases down to $|\mathbf{E}| \simeq 1.1$ μV/m for $L = 200$ km, $|\mathbf{E}| \simeq 0.6$ μV/m for $L = 100$ km, $|\mathbf{E}| \simeq 0.4$ μV/m for $L = 60$ km, and $|\mathbf{E}| \simeq 0.2$ μV/m for $L = 25$ km. Thus, an unbalanced current of 10 A can produce PLE with amplitude ∼6−12 μV/m above large scale (100–200 km) power lines. A high conductivity of the underlying crust can decrease the power emitted into the ionosphere. For example, a two orders of magnitude decrease of the crust resistivity would diminish the amplitude of the electromagnetic response in the upper ionosphere by about order of magnitude (Fedorov et al., 2020). Nonetheless, PLE with amplitudes about few μV/m were regularly detected by electric sensor onboard DEMETER and Chibis-M satellites (see references in review (Pilipenko, 2021)).

4.4. Generation of Artificial Pc1 Pulsations by Ground Power Lines

ULF waves in the Hz-frequency range (Pc1 pulsations) are of special significance for space physics. Through the resonant wave-particle interactions, electromagnetic ion-cyclotron waves in the Pc1 band can precipitate magnetospheric relativistic electrons into the atmosphere. Thus, intense Pc1 pulsations can suppress the natural or artificial radiation belts. Therefore, the idea emerged to stimulate the excitation of artificial Pc1 pulsations with the use of the radio heating facilities, for example, HAARP or Sura (see review of Guo et al. (2021)). However, the modulated heating of the ionosphere demands a high cost of construction and maintenance of radio-heating facilities. At the same time, an experiment with power transmission line as a controlled source of ULF emissions with the driving current up to 10^3 A can be easily implemented (Boerner, 1992). Power line generated artificial signals in the 1 Hz frequency range were detected on the ground over distances of more than 1,500 km, and such distances were never reported in the case of heating experiments (Ermakova et al., 2006).

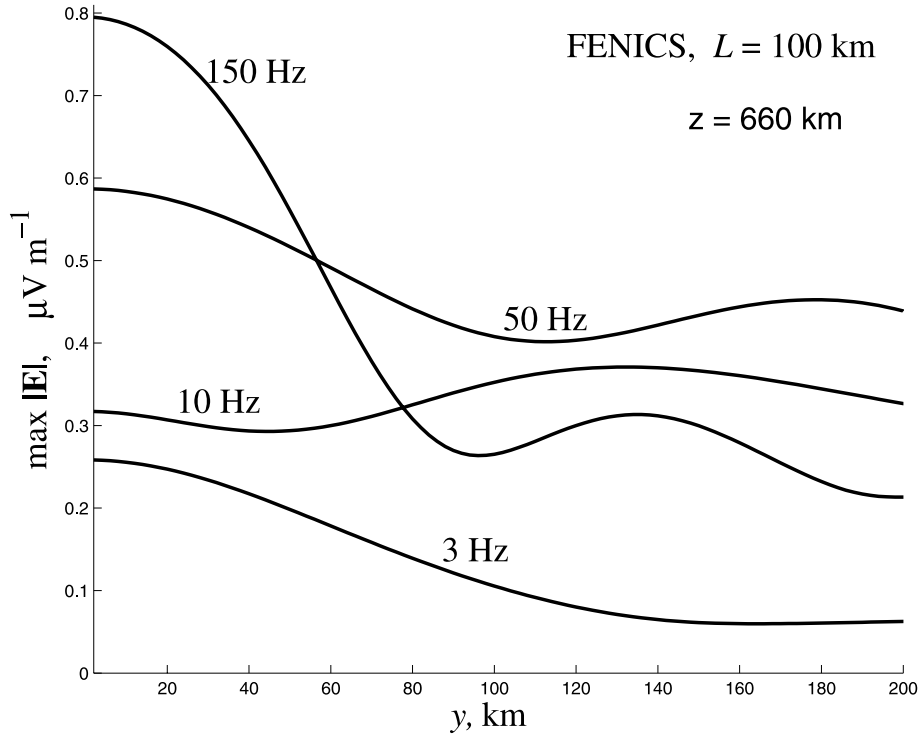

Figure 5. The radial structure of the extremely-low-frequency (ELF) emission intensity (electric component) in the upper ionosphere above the Fennoscandian Electrical conductivity from soundings with the Natural and Controlled Sources (FENICS) installation ($L = 100$ km) in the direction across antenna ($\phi = \pi/2$) for various emission frequencies.

Let us consider in greater detail the ionospheric response to the ground power line in the Pc1 frequency band, 0.5 Hz. Figure 7 (upper panel) shows the spatial structure of amplitudes of magnetic components excited by ground linear current in the direction across antenna. Amplitudes of the transverse magnetic components above a source are $B_y \sim 7 \cdot 10^{-3}$ pT and $B_x \sim 4 \cdot 10^{-3}$ pT. The compressional magnetic component reaches magnitude $B_z \sim 6 \cdot 10^{-3}$ pT at distance ∼400 km away from the source vertical. The occurrence of compressional component signifies that besides upward propagating emission, excitation of the ionospheric waveguide takes place.

Figure 7 (bottom panel) shows the spatial structure of amplitudes of transverse electric components excited by a linear current in the direction across the antenna. Amplitudes of the transverse electric components above a source are $E_y \sim 0.07$ μV/m, and $E_x \sim 0.01$ μV/m. At distances ∼200 km both components drop to magnitudes ≤0.01 μV/m.

Our modeling has shown that an installation with scale >100 km and current >140 A is sufficient under favorable conditions to stimulate emission in the Pc1 band (0.5 Hz) with amplitude ∼1 pT and ∼10 μV/m. Such amplitudes are typical for natural Pc1 signals in the upper ionosphere. Therefore, a power line, similar to the FENICS installation, at a latitude corresponding to the central part of the outer radiation belt can be used as a tool to deplete the relativistic electrons. An installation with a larger scale would be more efficient; for example, the emission from 200 km current is about 2 times larger than that from 100 km current. The use of large decommissioned power lines, where the AC up to 10^3 A can be easily generated, could be a cheap alternative to radio heating methods.

5. Discussion

The developed theoretical model predicts that in the upper nightside ionosphere above a 50–80 Hz transmitter with $L = 60$–100 km driven by 200 A current, the electric component with maximal amplitude up to ∼60−160 μV/m may be expected. This modeling result corresponds to the most favorable conditions, when a

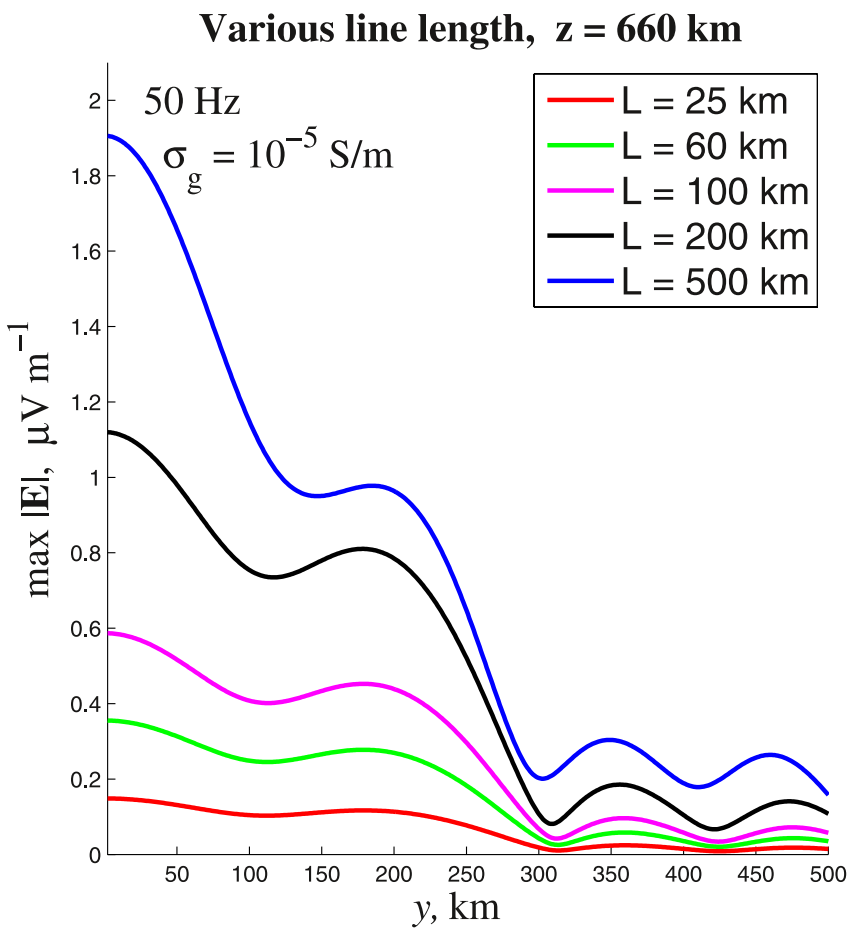

Figure 6. The radial structure of the electric component magnitude max|**E**| of 50 Hz emission in the upper ionosphere in the direction across antenna for different linear scales of power transmission line with an unbalanced current $J_0 = 1$ A.

satellite is exactly above the source, a high resistive underlying crust, and nighttime ionosphere. The modeling in Fedorov et al. (2020) with an infinite source showed a larger absorption of ELF emission in the daytime ionosphere as compared with nighttime conditions, though the difference was not very large. At an arbitrary mid-latitude location the vertical Poynting flux of the electromagnetic wave energy at 50 Hz for nighttime (00 LT) was about 35% larger than during daytime (12 LT). Therefore, the presented modeling results for nighttime conditions may be decreased about 40% for the daytime conditions. A similar dependence is expected for seasonal variations, whereas the favorable penetration conditions are expected in winter season. Nonetheless, even if the observational conditions are not optimal, still there are high chances to detect a response in the upper ionosphere to a ground large-scale emitter. The amplitude of exited ELF response decays with distance rather slowly, so it can be detected in a region with a radius of about several hundred km.

The developed model has some other limitations, for example, the geomagnetic field has been assumed to be vertical. However, the account for a finite geomagnetic field inclination will not modify the results considerably (Fedorov et al., 2021). The geomagnetic field can provide some guidance of ELF emission, so, as a result, an equatorward shift of maximum response in the ionosphere should be observed.

The assumption about an infinite line current provided somewhat overestimated maximal effects as compared with a finite length model. According to Figure 6, for 50 Hz emission the overestimate amounts to ~5.3 times for $L = 60$ km, ~3.3 times for $L = 100$ km, and ~1.7 times for $L = 200$ km. Away from the source ($\rho > 200$ km) the difference between the results of both models becomes small.

In a balanced three-phase power transmission system, the phase voltages should be equal. Even minor imbalance (asymmetry) of the phase voltages degrades the performance and shortens the lifetime of three-phase

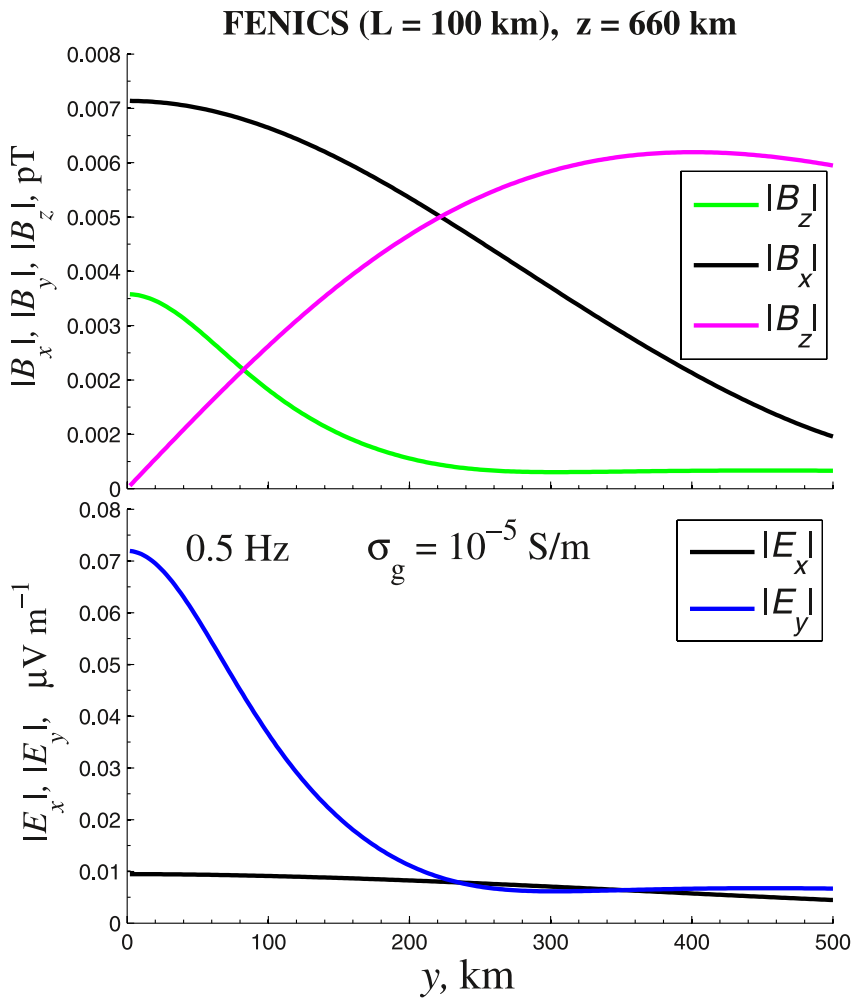

Figure 7. The radial structure of the amplitude of magnetic components $B_x(y)$, $B_y(y)$, $B_z(y)$ and horizontal electric components $E_x(y)$, $E_y(y)$ excited by ground linear transmitter with $L = 100$ km at $f = 0.5$ Hz in the direction across antenna.

loads. In general, current and voltage asymmetry reduces the efficiency of generation, transmission, and distribution of electricity (Koch et al., 2007). Whether GICs can induce an additional asymmetry in the operation of power transmission line is an unresolved problem. The observations of PLE in the near-Earth space indicate that on a global scale the existing power transmission lines operate in an unbalanced regime. The PLE amplitudes augmented with a modeling transmission coefficient may be considered as a global measure of such imbalance.

6. Conclusions

We have numerically estimated the penetration into the realistic ionosphere of ULF/ELF emission from a ground source modeled as a finite-scale linear current. The modeling shows that 10–150 Hz signals from a 60–100 km length source with current intensity 100–200 A can be reliably detected by electric sensors onboard the LEO satellites. The modeling confirms that power transmission lines and rail systems can be a source of PLE leaking into the upper ionosphere. We propose that decommissioned power lines can be used as an alternative tool to stimulate Pc1 pulsation activity in the ionosphere-magnetosphere system.

Data Availability Statement

The program may be requested from Rospatent Agency (registration ID 2023667115). Direct link is http://new.fips.ru/registers-doc-view/fips_servlet?DB=EVM&DocNumber=2023667115&TypeFile=html.

Acknowledgments
The study is supported by Grant 21-77-30010 from the Russian Science Foundation.

References

Bannister, P. R., Williams, F. J., Dahlvig, A. L., & Kraimer, W. A. (1974). Wisconsin Test Facility transmitting antenna pattern and steering measurements. *IEEE Transactions on Communications*, *22*(4), 412–418. https://doi.org/10.1109/tcom.1974.1092224

Belyaev, P. P., Polyakov, S. V., Ermakova, E. N., Yakunin, M. N., Sobchakov, L. A., Vasilyev, A. V., et al. (2002). First experiments on generation and receiving artificial ULF (0.3–12) Hz emissions at a distance of 1500 km. *Radiophysics Quantum Electronics*, *46*(12), 135–146. https://doi.org/10.1023/A:1015949625839

Bernstain, S. L., Barrouz, M., Evans, D. E., Griffits, E. S., Macneil, D. A., Nissen, C. U., et al. (1974). Distant communication on extremely low frequencies. *Proceedings of the IEEE*, *62*, 5–30.

Bilitza, D., Pezzopane, M., Truhlik, V., Altadill, D., Reinisch, B. W., & Pignalberi, A. (2022). The international reference ionosphere model: A review and description of an ionospheric benchmark. *Reviews of Geophysics*, *60*(4), e2022RG000792. https://doi.org/10.1029/2022RG000792

Boerner, D. E. (1992). Controlled source electromagnetic deep sounding: Theory, results and correlation with natural source results. *Surveys in Geophysics*, *13*(4–5), 435–488. https://doi.org/10.1007/bf01903486

Budden, K. G. (1985). *The propagation of radio waves*. Cambridge University Press.

Ermakova, E. N., Kotik, D. S., Polyakov, S. V., Bosinger, T., & Sobchakov, L. A. (2006). A power line as a tunable ULF-wave radiator: Properties of artificial signal at distances of 200 to 1000 km. *Journal of Geophysical Research*, *111*(A4), A04305. https://doi.org/10.1029/2005JA011420

Ermakova, E. N., Ryabov, A. V., & Kotik, D. S. (2021). Features of the spectra of ultralow-frequency magnetic fields from horizontal current sources: Models of plane and spherical waveguides earth-ionosphere. *Radiophysics Quantum Electronics*, *64*(N3), 163–178. https://doi.org/10.52452/00213462_2021_64_03_163

Fedorov, E. N., Mazur, N. G., & Pilipenko, V. A. (2021). Electromagnetic response of the mid-latitude ionosphere to power transmission lines. *Journal of Geophysical Research: Space Physics*, *126*(10), e2021JA029659. https://doi.org/10.1029/2021JA029659

Fedorov, E. N., Mazur, N. G., & Pilipenko, V. A. (2023). Electromagnetic field in the upper ionosphere from horizontal ELF ground-based transmitter with a finite length. *Radiophysics and Quantum Electronics*, *65*(N9), 697–712. https://doi.org/10.1007/s11141-023-10245-z

Fedorov, E., Mazur, N., Pilipenko, V., & Baddeley, L. (2016). Modeling the high-latitude ground response to the excitation of the ionospheric MHD modes by atmospheric electric discharge. *Journal of Geophysical Research: Space Physics*, *121*(11), 11282–11301. https://doi.org/10.1002/2016JA023354

Fedorov, E., Mazur, N., Pilipenko, V., & Vakhnina, V. (2020). Modeling ELF electromagnetic field in the upper ionosphere from power transmission lines. *Radio Science*, *121*(7), e2019RS006943. https://doi.org/10.1029/2019RS006943

Fraser-Smith, A. C., & Coates, D. B. (1978). Large-amplitude ULF electromagnetic fields from BART. *Radio Science*, *13*(4), 661–668. https://doi.org/10.1029/RS013i004p00661

Guo, Z., Fang, H., & Honary, F. (2021). The generation of ULF/ELF/VLF waves in the ionosphere by modulated heating. *Universe*, *7*(2), 29. https://doi.org/10.3390/universe7020029

Inan, U. S., Cummer, S. A., & Marshall, R. A. (2010). A survey of ELF and VLF research on lightning-ionosphere interactions and causative discharges. *Journal of Geophysical Research*, *115*(A6), A00E36. https://doi.org/10.1029/2009JA014775

Koch, R. G., Beaulieu, G., Berthet, L., & Halpin, M. (2007). International survey of unbalance levels in LV, MV, HV, and EHV power systems. In *CIGRE/CIRED JWG C4.103 Results. Paper 0892*. CIRED.

Kostrov, A. V., Gushchin, M. E., & Strikovskii, A. V. (2017). Generation and radiation of high power line harmonics. *Geomagnetism and Aeronomy*, *57*(4), 482–490. https://doi.org/10.1134/S0016793217030094

Mazur, N. G., Fedorov, E. N., Pilipenko, V. A., & Vakhnina, V. V. (2018). ULF electromagnetic field in the upper ionosphere excited by lightning. *Journal of Geophysical Research: Space Physics*, *123*(8), 6692–6702. https://doi.org/10.1029/2018JA025622

Nemec, F., Parrot, M., & Santolik, O. (2015). Power line harmonic radiation observed by the DEMETER spacecraft at 50/60 Hz and low harmonics. *Journal of Geophysical Research: Space Physics*, *120*(10), 8954–8967. https://doi.org/10.1002/2015ja021682

Nemec, F., Santolik, O., Parrot, M., & Bortnik, J. (2008). Power line harmonic radiation observed by satellite: Properties and propagation through the ionosphere. *Journal of Geophysical Research*, *113*(A8), A08317. https://doi.org/10.1029/2008ja013184

Nickolaenko, A. P., Shvets, A. V., & Hayakawa, M. (2016). Extremely low frequency (ELF) radio wave propagation: A review. *International Journal of Electronics and Applied Research*, *3*(2), 81.

Parrot, M. (2018). DEMETER observations of manmade waves that propagate in the ionosphere. *Comptes Rendus Physique*, *19*(1–2), 26–35. https://doi.org/10.1016/j.crhy.2018.02.001

Pilipenko, V. A. (2021). Space weather impact on ground-based technological systems. *Solar-Terrestrial Physics*, *7*(N3), 68–104. https://doi.org/10.12737/stp-73202106

Pilipenko, V. A., Fedorov, E. N., Mazur, N. G., & Klimov, S. I. (2021). Electromagnetic pollution of near-earth space by radiation from power lines. *Solar-Terrestrial Physics*, *7*(N3), 3–12. https://doi.org/10.12737/szf-71202101

Pilipenko, V. A., Parrot, M., Fedorov, E. N., & Mazur, N. G. (2019). Electromagnetic field in the upper ionosphere from ELF ground-based transmitter. *Journal of Geophysical Research: Space Physics*, *124*(10), 8066–8080. https://doi.org/10.1029/2019JA026929

Rothkaehl, H., & Parrot, M. (2005). Electromagnetic emissions detected in the topside ionosphere related to the human activity. *Journal of Atmospheric and Solar-Terrestrial Physics*, *67*(8–9), 821–828. https://doi.org/10.1016/j.jastp.2005.02.003

Sobchakov, L. A., Astakhova, N. L., & Polyakov, S. V. (2003). Excitation of electromagnetic waves in a plane waveguide with an anisotropic upper wall. *Radiophysics Quantum Electronics*, *46*(N12), 918–927. https://doi.org/10.1023/b:raqe.0000029586.85070.9b

Starks, M. J., Quinn, R. A., Ginet, G. P., Albert, J. M., Sales, G. S., Reinisch, B. W., & Song, P. (2008). Illumination of the plasmasphere by terrestrial very low frequency transmitters: Model validation. *Journal of Geophysical Research*, *113*(A9), A09320. https://doi.org/10.1029/2008JA013112

Tereshenko, E. D., & Tereshenko, P. E. (2017). Electric field of horizontal linear water-grounded aerial. *Journal of Technical Physics*, *87*, 453–457.

Velikhov, E. P., Zhamaletdinov, A. A., Shvetsov, A. N., Tokarev, A. D., Kononov, Y. M., Pesin, L. B., et al. (1998). Deep electromagnetic studies with the use of powerful ELF radio installations. *Physics of the Solid Earth*, *34*(N8), 615–632.

Velikhov, Y. P., Zhamaletdinov, A. A., Sobchakov, L. A., Veshev, A. V., Saraev, A. K., Tokarev, A. D., et al. (1994). Experiment on the frequency electromagnetic sounding of the Earth crust with the use of the powerful ELF antenna. *Doklady Akademii Nauk*, *338*(N1), 106–109.

Wait, J. R. (1972). *Electromagnetic waves in stratified media* (p. 372). Elsevier.

Wu, J., Fu, J. J., & Zhang, C. (2014). Propagation characteristics of power line harmonic radiation in the ionosphere. *Chinese Physics B*, *23*, 034102–034107. https://doi.org/10.1088/1674-1056/23/3/034102

Wu, J., Guo, Q., Yan, X., & Zhang, C. (2019). Theoretical analysis on affecting factors of power line harmonic radiation. *IEEE Transactions on Plasma Science*, *47*(1), 770–775. https://doi.org/10.1109/TPS.2018.2865827

Wu, J., Guo, Q., Yue, C., Xie, L., & Zhang, C. (2019). Special electromagnetic interference in the ionosphere directly correlated with power system. *IEEE Transactions on Electromagnetic Compatibility*, *62*(3), 947–954. https://doi.org/10.1109/TEMC.2019.2918280

Wu, J., Zhang, J., & Xie, L. (2022). Uncommon electromagnetic radiations related to extra-high voltage/ultra-high voltage power projects in China. *Frontiers of Environment Science*, *10*, 902508. https://doi.org/10.3389/fenvs.2022.902508

Zhamaletdinov, A. A., Shevtsov, A. N., Velikhov, E. P., Skorokhodov, A. A., Kolesnikov, V. E., Korotkova, T. G., et al. (2015). Study of interaction of ELF-ULF range (0.1–200 Hz) electromagnetic waves with the Earth's crust and the ionosphere in the field of industrial power transmission lines (FENICS experiment). *Izvestiya - Atmospheric and Oceanic Physics*, *51*(8), 826–857. https://doi.org/10.1134/s0001433815080083

Zhang, C., & Ma, Q. (2018). Influences of radiation from terrestrial power sources on the ionosphere above China based on satellite observation. *2nd International Workshop on Renewable Energy and Development, Conference Series: Earth and Environmental Science*, *153*, 042002. https://doi.org/10.1088/1755-1315/153/4/042002